Theoretical Chemistry Accounts (2018) 137:128
https://doi.org/10.1007/s00214-018-2318-9

REGULAR ARTICLE

Structures and stability of adsorbed methanol on TiO_2(110) surface studied by ab initio thermodynamics and kinetic Monte Carlo simulation

Keju Sun[1] · **Hai-Yan Su**[2] · **Wei-Xue Li**[3]

Received: 10 June 2018 / Accepted: 21 September 2018 / Published online: 27 September 2018

Abstract
The structures and stability of adsorbed methanol on TiO_2(110) surface have been extensively studied because of its application for direct hydrogen production and promoting hydrogen production in photocatalysis. In this work, combined with ab initio thermodynamics and kinetic Monte Carlo (KMC), a detailed microscopic picture of methanol adsorption structure on TiO_2(110) surface at different conditions is mapped out for the first time. The thermodynamics analysis based on the density functional theory calculations shows that the methanol adsorption at coverage of 2/3 ML is prevailed at a very wide range of temperatures and pressures. The simulated temperature-programmed desorption (TPD) based on KMC indicates that the full monolayer adsorption methanol desorbs at about 150 K and the methanol dimer at a coverage of 2/3 ML is stable up to 250 K. At higher temperature, the methanol dimer becomes unstable and decomposes to the monomer, which desorbs from the surface at 350 K. The present simulated results agree well with the experimental TPD results.

Keywords Methanol adsorption · TiO_2(110) surface · Ab initio thermodynamics · Kinetic Monte Carlo · Temperature-programmed desorption simulation

1 Introduction

The structures and stability of methanol on TiO_2 have received wide attention because of its potential application in photocatalysis [1]. The methanol could not only produce hydrogen by itself, but also promote hydrogen production from water [2–5]. Due to the importance of methanol in photocatalyzed hydrogen production, a number of experimental and theoretical studies have been performed to investigate the methanol adsorption and its role on TiO_2 [4, 6–8]. Despite the numerous studies, the fundamental adsorbed structures of methanol on TiO_2 remain unclear [9], which increase the difficulty in the study of photocatalytic reaction mechanism.

For instance, Onishi et al. [10] reported that no ordered overlayer of methanol on TiO_2(110) surface was observed based on LEED pattern. However, Henderson et al. [11, 12] identified a coverage of 2/3 ML methanol from a weak and streaky LEED pattern, and a corresponding structural model with both methoxy and methanol was proposed. Theoretical calculations mainly focused on the configurations of methanol on TiO_2(110) at different coverages [13, 14] or on different surfaces including stoichiometric and defective surface [15, 16]. So far as we know, the structures of adsorbed methanol on TiO_2(110) surface as a function of reaction conditions are not available.

In this work, the stabilities of methanol adsorption on TiO_2(110) surface under wide range of coverages are investigated, taking into account the effect of temperatures and pressures. The phase diagram of methanol on TiO_2(110) surface was achieved to obtain the adsorption structure at the thermodynamic equilibrium. To find the adsorption structure of methanol on TiO_2(110) surface at non-thermodynamic

✉ Keju Sun
kjsun@ysu.edu.cn

✉ Wei-Xue Li
wxli70@ustc.edu.cn

[1] Key Laboratory of Applied Chemistry, College of Environmental and Chemical Engineering, Yanshan University, Qinhuangdao 066004, China

[2] State Key Laboratory of Molecular Reaction Dynamics, Dalian Institute of Chemical Physics, Chinese Academy of Sciences, Dalian 116023, China

[3] Department of Chemical Physics, iChEM, University of Science and Technology of China, Hefei 230026, China

equilibrium, the kinetic Monte Carlo simulation was performed to simulate the temperature-programmed desorption of methanol on TiO_2(110) surface.

It is found that the structure with 2/3 ML methanol is the thermodynamically most favorable structure after annealing at 200 K, which is a dimer structure and formed via the competitive interaction between adsorbate–substrate, hydrogen bond and steric repulsion of methyls. It should be noted that the 1 ML coverage means the ratio of adsorbed methanol to surface fivefold titanium to be one, which is different from the traditional saturated concept.

2 Computational methods

2.1 Density functional theory calculations

Periodic density function theory (DFT) calculations have been performed using the Vienna Ab Initio Simulation Package (VASP) [17]. The total energy was calculated by solving the Kohn–Sham equations, using the exchange–correlation functional proposed by Perdew and Zunger [18] corrected for non-locality in the generalized gradient approximation with PW91 functional [19]. VASP uses plane waves to expand wave functions, PAW potentials, [20] allowing a significant reduction of the number of plane waves. For the present calculations, a cutoff of 400 eV has been used. The relaxation ions in the super cell are relaxed until the residual force on each ion is less than 0.02 eV $Å^{-1}$. The vacuum layer is larger than 15 Å. The K points mesh was set by Monkhorst–Packing methods as $2\times4\times1$ for TiO_2(110) surface. The optimized lattice constants of bulk rutile TiO_2 are $a=4.664$ Å and $c=2.967$ Å, in good agreement with the experimental values ($a=4.594$ Å and $c=2.958$ Å) [21]. The effect of spin polarization is tested, and it is found that the influence of spin polarization on total energy is less than 0.01 eV and therefore neglected in the present calculations.

The calculated surface energy of TiO_2(110) surface is 0.0367 eV $Å^{-2}$, slightly higher than the previous DFT value of 0.035 eV $Å^{-2}$ [22]. Considering the different potential (PAW potentials and ultrasoft pseudopotentials) and the energy of cutoff (400 eV and 495 eV) used, our results agree closely with previous calculations. To obtain the influence of different functional, the adsorbed molecular and dissociated methanol on (4×1)-TiO_2(110) surface on the 6-trilayer slab was calculated by PW91 functional, with DFT-D3(Becke–Johnson) correction method [23, 24] and hybrid HSE06 functional. The calculated adsorption energies of molecular methanol are -85.5, -113.2 and -86.1 kJ mol^{-1}, and those of dissociated methanol are -90.8, -115.9 and -97.7 kJ mol^{-1} by PW91 functional, with DFT-D3(Becke–Johnson) correction method and hybrid HSE06 functional, respectively. Compared to hybrid HSE06 functional, the PW91 functional slightly underestimates the adsorption, while DFT-D3 correction overestimates the adsorption. The agreement of the results from PW91 functional and HSE06 functional shows that the PW91 functional is a good functional to describe the TiO_2 surface.

2.2 Thermodynamical analysis

Based on the calculated total energy (enthalpy) by DFT calculation, the chemical potential is calculated. The chemical potential of gaseous methanol (μ_{methanol}) is written as:

$$\mu_{\text{methanol}} = E_{\text{methanol}} + \Delta\mu_{\text{methanol}}(T,p) \tag{1}$$

where E_{methanol} is the total energy of the methanol molecule, and $\Delta\mu_{\text{methanol}}(T, p)$ includes the contribution from translations, rotations, vibrations of methanol molecule at the pressure (p) and temperature (T) and normally is defined as

$$\begin{aligned}\Delta\mu_{\text{methanol}}(T,p) = &-RT\ln\frac{(2\pi mkT)^{3/2}}{h^3}\\ &-RT\ln kT + RT\ln p\\ &-RT\ln\left(\frac{8\pi^2(2\pi kT)^{3/2}}{\sigma h^3}(I_x\cdot I_y\cdot I_z)^{1/2}\right)\\ &-RT\ln\left(\prod_{i=1}^{3n-6}\frac{e^{-\frac{h\nu_i}{2kT}}}{1-e^{-\frac{h\nu_i}{kT}}}\right)\end{aligned} \tag{2}$$

where R, m, k, h, I_x, I_y, I_z, σ and $\nu_{i(i=1,2,\ldots,12)}$ are the gas constant, the molecular mass of methanol, Boltzmann constant, Planck constant, the rotational inertia of methanol in the direction of x, y and z, the rotational symmetry number and the vibration frequency of methanol, respectively. The values of m and σ for methanol are 5.314×10^{-26} kg and 1, respectively. It should be noted that the values of I_x, I_y and I_z depend on the selected coordinate origin and direction, and the used values are 6.6496×10^{-47} kg m^2, 3.1520×10^{-46} kg m^2 and 3.4197×10^{-46} kg m^2, respectively. The calculated $\nu_{i(i=1,2,\ldots,12)}$ are 3746.1, 3056.2, 2983.2, 2912.9, 1465.7, 1451.4, 1431.5, 1329.6, 1137.1, 1055.7, 1013.1, 294.8 cm^{-1}, respectively.

The surface Gibbs free energy of methanol on the TiO_2(110) surface ($\Delta G_{\text{methanol}}$) is defined as following:

$$\Delta G_{\text{methanol}} = G_{\text{surf+methanol}} - G_{\text{surf}} \tag{3}$$

where $G_{\text{surf+methanol}}$ and G_{surf} are the surface Gibbs free energy of TiO_2 surface with and without the adsorbed methanol.

The surface Gibbs free energy can be decomposed into several contributing terms

$$G = E^{\text{total}} + F^{\text{vib}} + F^{\text{conf}} + pV \tag{4}$$

where E^{total} is the inner energy from DFT calculations. According to the Debye model,

$$F^{\mathrm{vib}} = -RT \ln \prod_{i=1}^{3n} \frac{e^{-\frac{1}{2}\frac{h\nu_i}{kT}}}{1 - e^{-\frac{h\nu_i}{kT}}} \tag{5}$$

The calculated $\nu_{i(i=1,2,\ldots,18)}$ of methanol on TiO_2(110) surface are 3267.3, 3103.0, 3046.3, 2948.7, 1464.7, 1447.1, 1423.6, 1324.3, 1141.5, 1115.0, 1000.9, 775.9, 559.0, 537.8, 371.4, 344.5, 292.4, 257.0 cm^{-1}, respectively. The contribution of F^{conf} and pV terms is rather small in most cases [25] and thus are ignored in this work.

2.3 Kinetic Monte Carlo simulation

The kinetic Monte Carlo (KMC) simulation can be used to explicitly track individual molecular transformations as functions of time and processing conditions, and the details have been described in references [26–31]. A general flowchart of the traditional KMC is shown in Fig. 1. The first step of the traditional KMC is initialization of the parameters, such as initial temperature, heating rate and coverage. Then, the rates of all events including desorption from the surface and the diffusion on the surface are calculated. The reaction rate (r_i) of each event is normally defined by the transition state theory, as follows

$$r_i = A_i \exp\left(-\frac{\Delta E_i}{RT}\right) \tag{6}$$

where A_i is the pre-exponential factor and ΔE_i is the activation barrier for the event i. Subsequently, the time step (Δt) at which one event will occur is calculated as,

$$\Delta t = -\frac{\ln\left(R_N\right)}{\sum_i^N r_i} \tag{7}$$

where R_N is a random number between 0 and 1. After the time step calculations, one event is chosen to occur based on the probability

$$P_i = \frac{r_i}{\sum_i^N r_i} \tag{8}$$

Then, time, temperature, surface structure, surface composition and gas-phase products are updated, and the total time is updated by adding Δt to the current time. Finally, it is a step to decide if the cycle needs to continue. If the result achieves the target (in this work, $T > T_{\mathrm{end}}$), the cycle will end. Otherwise, the traditional KMC will go back to the second step of the recycle to recalculate the rates of all events.

From Eq. (8), it can be found that the P_i of an event is proportional to its reaction rate (r_i). Therefore, P_{i} of the fast process with high reaction rate is higher than that of slow process. As a result, most of the time in traditional KMC theory is used to simulate fast processes. However, the key step is slow process instead of fast process in most case. In present work, the diffusion barrier of methanol on TiO_2 is calculated to be 50.6 kJ mol^{-1} at 1/4 ML coverage using the force reversed method [32], and the corresponding desorption barrier is 85.3 kJ mol^{-1}. According to Eq. (6), the diffusion process of methanol is several orders of magnitude faster than methanol desorption from TiO_2(110) surface. Specially, the diffusion process is six orders of magnitude faster than the desorption process at 300 K. As a result, the traditional KMC simulation spends too much time (99.9999% time) in simulating the diffusion process, and only about 0.0001% time is left in simulating the real key

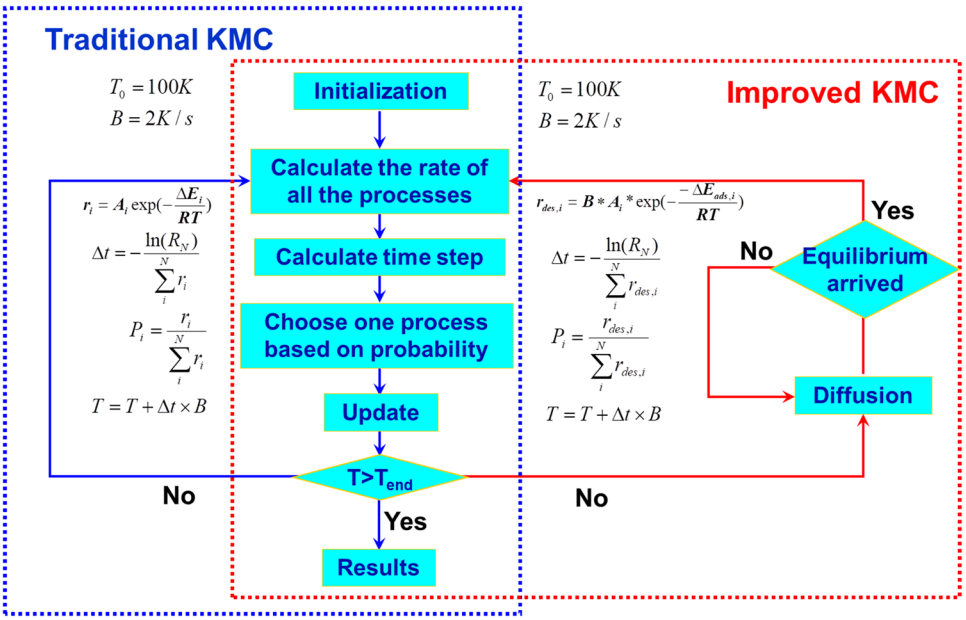

Fig. 1 Flowchart of the traditional KMC in blue-dotted rectangle and the improved KMC methods in red-dotted rectangle

step of the desorption process. The computation efficiency is thus greatly decreased in traditional KMC theory. Aiming to overcome this shortcoming, we improve the KMC simulation method in this work.

Since the diffusion process is much faster than the desorption process, we can assume that each desorption process of methanol occurs only if diffusion equilibrium of methanol on TiO_2(110) is achieved. Based on this assumption, we can treat diffusion process and desorption process separately, as shown in the improved KMC simulation in Fig. 1. Only the desorption processes are considered as the events in main KMC simulation, and the diffusion process is so fast compared to desorption process that the elapsed time of diffusion process is ignored. The thermodynamics diffusion equilibrium is achieved by using Monte Carlo simulation based on the thermodynamic probability

$$P_{\mathrm{diff},\, i\to j} = \frac{\mathrm{e}^{-\Delta E_{\mathrm{diff},i\to j}/RT}}{1+\mathrm{e}^{-\Delta E_{\mathrm{diff},\, i\to j}/RT}} \tag{9}$$

where $P_{\mathrm{diff},\, i\to j}$ is the thermodynamic probability of methanol diffused from site i to the neighboring site j and the $\Delta E_{\mathrm{diff},\, i\to j}$ is the adsorption energy difference of methanol between site i and site j. Our tests indicate that the thermodynamic equilibrium is arrived after 100 surface diffusions on the periodic 24 × 24 surfaces in most cases. To obtain a reliability result, the each desorption of methanol molecule starts after 1000 surface diffusions in the improved KMC simulations. The flowchart of the improved KMC simulation is shown in Fig. 1.

The specific parameters used in the improved KMC simulation are described below. The TiO_2(110) surface is represented by a periodic 24 × 24 fivefold Ti sites. The intrinsic desorption activation barriers (ΔE_{ads}) are taken from the DFT results. Our DFT calculations show that the desorption activation barrier is almost equal to the desorption energy (negative adsorption energy), and therefore, the negative adsorption energy is defined as the desorption activation barrier. As a result, the desorption rate for each elementary step is given by

$$r_{\mathrm{des},i} = B * A_i * \exp\left(-\frac{-\Delta E_{\mathrm{ads},i}}{RT}\right) \tag{10}$$

where B is the heating rate of 2 K s^{-1} and the pre-exponential factor A_i is used as 10^{13} s^{-1} in present work. It should be noted that the simulated results were not significantly affected by changes in B and A_i [29]. Our simulation results show that the desorption peak will shift about 20 K to higher temperature when the value of $B * A_{\mathrm{i}}$ is decreased with a factor of ten. The final simulated TPD process was obtained from a sum of 100 simulations.

It should be noted that the dissociation barrier of methanol on TiO_2(110) surface at 1/4 ML coverage is calculated to be 18.3 kJ mol^{-1} and the corresponding barrier of the reverse process from the dissociated methanol is 23.6 kJ mol^{-1}, much lower than the diffusion barrier of 50.6 kJ mol^{-1} and the desorption barrier of 85.3 kJ mol^{-1}. Therefore, the dissociation process and corresponding reverse process of methanol on TiO_2(110) surface are so fast compared to the diffusion and desorption that the dissociation process and the corresponding reverse process achieve equilibrium and can be ignored in the work.

3 Results

It is well known that the adsorption energy of adsorbates on TiO_2(110) surface converges concussively with the thickness of slab layer. To obtain a full convergence, we calculated the dependence of the energy difference between the molecular and dissociated methanol on (4 × 1)-TiO_2(110) surface on the slab thickness. Full relaxation for all ions and partial relaxation (the ions in the bottom two trilayers are frozen to the bulk-truncated positions) were considered, and the calculated adsorption energy differences between molecular adsorption and dissociated adsorption as a function of slab thickness are shown in Fig. 2a. Compared to the full relaxation, where the energy difference is not converged even for eight- and nine-layer slabs, it converges quickly for the partial relaxation. Assuming the average energy difference from eight- and nine-layer slabs of full relaxation as the converged value, the model of six-layer slabs for partial relaxation approaches the reasonable result. Thus, the six-layer slabs with the frozen two bottommost layer ions are used in the following calculations.

Two typical most stable structures of methanol adsorption on TiO_2(110) surface are shown in Fig. 3. Figure 3a displays the dissociative methanol monomer, where the dissociated hydrogen locates on the bridge oxygen and points to the oxygen of CH_3O group at neighboring Ti^{4+} site. Figure 3b shows the partial dissociative methanol dimer, where the hydrogen of the undissociated methanol at Ti^{4+} site points to the oxygen of dissociated methanol at neighboring Ti^{4+} site, forming a hydrogen bonding between two methanol molecules in the dimer. The hydrogen from the dissociative methanol locates on neighbor bridging oxygen and points to the oxygen of the dissociative methanol. The dissociative monomer and partial dissociative dimer are more stable than the corresponding molecular adsorption states by about 5–10 kJ mol^{-1} dependent on coverage, which is in good agreement with the DFT results by Liu et al. [33]. Correspondingly, the dissociative monomer and partial dissociative dimer are used in the following discussion unless otherwise indicated.

Figure 2b shows the calculated average adsorption energy of methanol monomer and dimer with respect to the coverage by DFT calculations. It is found that the adsorption

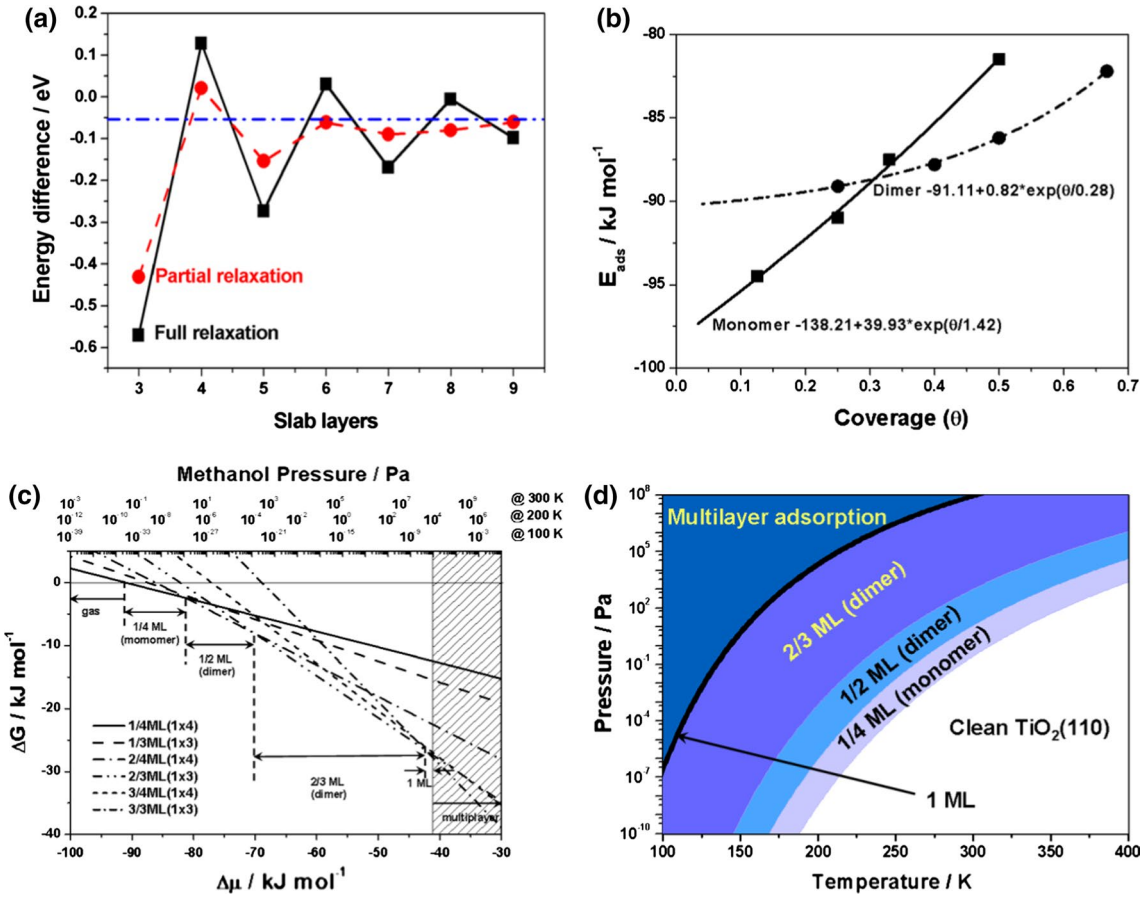

Fig. 2 **a** Dependence of the adsorption energy on the thickness of the slab at coverage of 1/4 ML. **b** The average adsorption energy of the methanol partly dissociated on TiO_2(110) surface at different coverage. **c** Free energy diagram for partly dissociative methanol adsorbed on TiO_2(110). **d** Calculated phase diagram for the methanol on TiO2(110) surface

energy of methanol increases with increasing coverages regardless of monomer and dimer. When the coverage is lower than 0.3 ML, the monomer structure is more stable than the dimer structure. However at higher coverages, the dimer becomes more favorable. The stability switch may originate from OH groups in methanol monomer at high coverages, leading to shorter average distance between the neighboring OH groups and strong repulsion interaction.

Based on the structures and energetics in Fig. 2b, we have constructed the surface free energy diagram in Fig. 2c for methanol adsorption on stoichiometric TiO_2(110) surface. The thermodynamic parameters of the gaseous methanol are described by the chemical potential Δμ. The methanol partial pressures corresponding to Δμ at a given temperature are also shown in Fig. 2c. The shaded part marks the range of Δμ where multilayer methanol (or liquid methanol) is thermodynamically favored. In Fig. 2c, we can find that the coverage of methanol on the TiO_2(110) surface increases with increasing pressures at the given temperature. For instance, when the pressure is lower than 10^{-10} Pa at 200 K, the gaseous methanol is the most stable. With increasing pressures to 10^{-10} Pa to 10^4 Pa, the methanol prefers to be monolayer adsorption at the coverage from 1/4 to 1 ML. At a pressure higher than 10^4 Pa, the multilayer methanol adsorption or liquid methanol is more favorable.

Based on the free energy diagram of Fig. 2c, the adsorbed structures as a function of temperature and pressure are considered, yielding the phase diagram in Fig. 2d. It is interesting to find that the 1 ML methanol adsorption structure is only stable in a very narrow range, and the 2/3 ML structure is preferential at a wide range of pressures and temperatures. The stability of 2/3 ML structure should be assigned to its unique structure as shown in Fig. 3c. The distance between two neighboring 5-coordinated surface Ti^{4+} is about 3.0 Å, while the diameter of methyl is 4.1 Å. Therefore, strong steric repulsion between the neighboring methyls occurs for high coverage of methanol. On the balance of the interaction between adsorbate–substrate, hydrogen bond and steric repulsion between methyls, the structure with 2/3 ML instead of that with 1 ML is preferential at a very wide range of temperatures and pressures. The lower coverage than 1 ML can also be expected for other alcohols such as ethanol

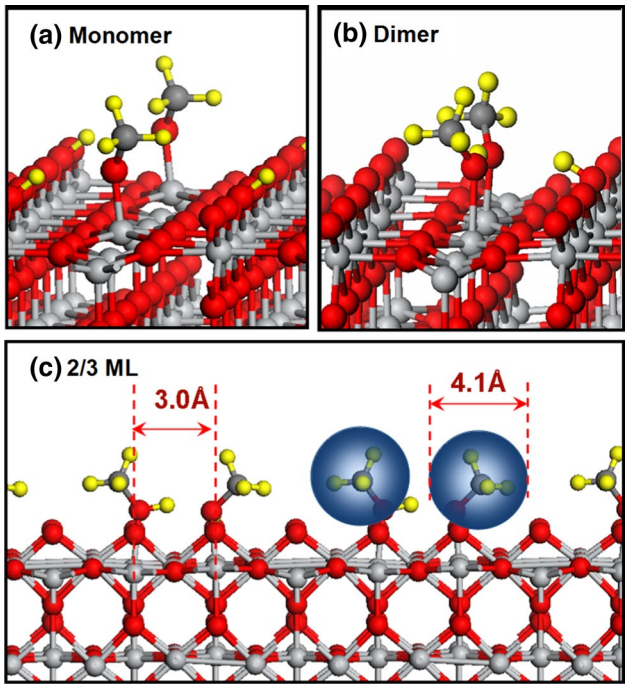

Fig. 3 Adsorption structures of methanol on TiO_2(110) surface with monomer adsorption (**a**), dimer adsorption (**b**) and the adsorption at 2/3 ML (**c**). The red, yellow, gray and silver balls denote the O, H, C, Ti atoms, respectively

and propanol adsorption on TiO_2(110) surface due to the steric repulsion.

Although the stable adsorption structure of methanol on TiO_2(110) surface can be identified at a given pressure and temperature in thermodynamic equilibrium from the phase diagram of Fig. 2d. Many surface experiments, such as temperature-programmed desorption (TPD), are measured at the non-thermodynamic equilibrium. To obtain the structure information of methanol adsorption on TiO_2(110) under non-thermodynamic equilibrium conditions, we simulate TPD from kinetic Monte Carlo from the initial coverages of 1 ML at 125 K to 0 ML at 375 K as shown in Fig. 4.

It is found that three desorption peaks appear at 155 K, 290 K and 350 K in Fig. 4, in good agreement with those at 165 K, 295 K and 350 K in the TPD experiment in Fig. 5a [11]. From the snapshots of adsorbed methanol molecules on TiO_2(110) surface at different temperatures, the peak at 155 K is assigned to the methanol desorption from 1 to 2/3 ML. At 200 K, most methanol molecules on the TiO_2(110) surface is transformed to stable dimer structure, with the corresponding coverage of 2/3 ML. The peak at 290 K is assigned to the desorption induced by the transformation from dimer structures to monomer structures. The peak at 350 K is assigned to the desorption of methanol monomer. Our simulations suggest that 2/3 ML methanol on TiO_2(110) surface is relative stable from 180 K to 250 K, which is in consistent with the results of TPD and LEED experiments by Henderson et al. [11].

Figure 5b shows the simulated TPD at initial coverage of partly dissociative methanol on surface Ti^{4+} from 0.1 to 1.0 ML and dissociated methanol on bridge oxygen vacancy with surface concentration of 10%. The corresponding adsorption energy of the dissociated methanol on bridge oxygen vacancy is calculated to be -133.9 kJ mol^{-1} at the coverage of 1/4 ML, much stronger than that on the 5-coordinated surface Ti^{4+} with -91.0 kJ mol^{-1}, which agrees well with the recent results [34]. Therefore, all the oxygen

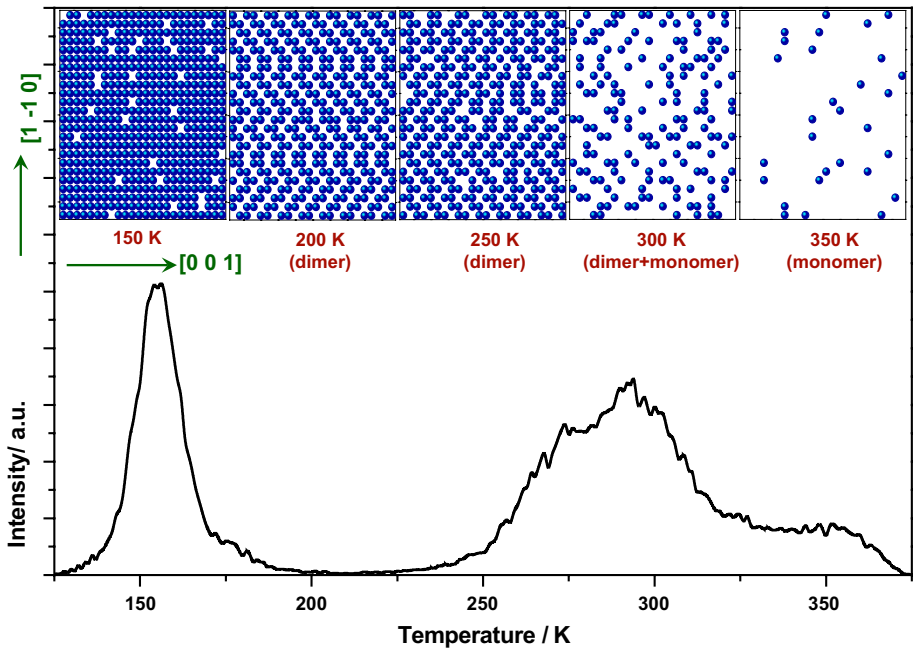

Fig. 4 Simulated TPD from kinetic Monte Carlo based on methanol partly dissociated on surface Ti^{4+} of TiO_2(110) surface (the bottom panel) and the snapshots of adsorbed methanol at different temperatures (the top panel). The initial coverage is 1 ML on surface Ti^{4+}

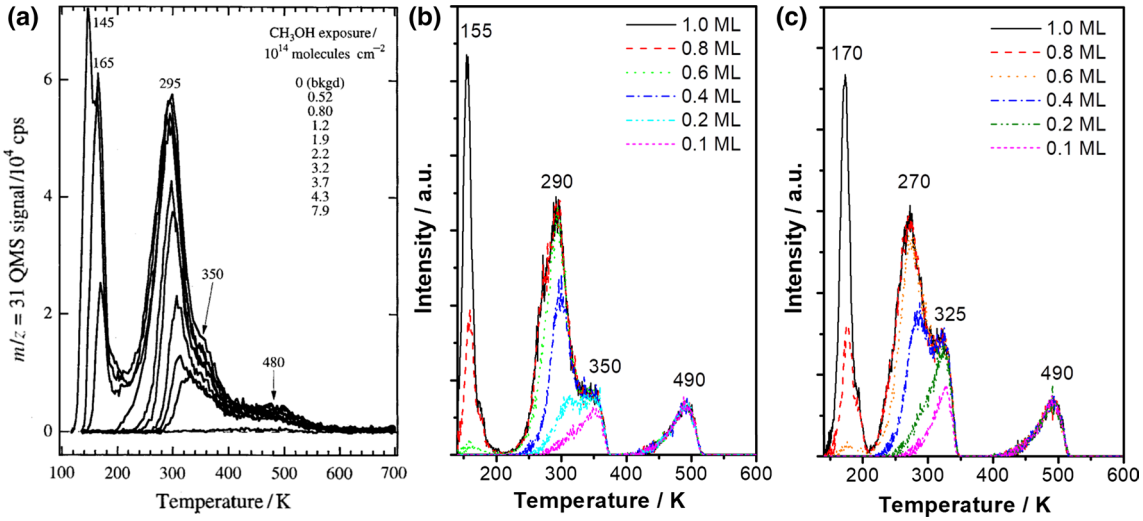

Fig. 5 Experimental CH_3OH ($m/z=31$) TPD spectra with different CH_3OH exposures on $TiO_2(110)$ surface by Henderson et al. [11] (**a**) and simulated TPD from kinetic Monte Carlo based on adsorbed partly dissociative methanol (**b**) and molecular methanol (**c**) at different coverage. The coverage of methanol is corresponding to the methanol on surface Ti^{4+}, and the concentration of oxygen vacancy is set to 10%

vacancies are occupied by dissociated methanol, if there are methanol on surface Ti^{4+} site. Based on KMC simulation, the desorption peak of dissociated methanol on bridge oxygen vacancy is predicted at about 490 K. This result is supported by the experimental TPD results, in which a desorption peak at 480 K is observed and assigned to the dissociated methanol on bridge oxygen vacancy as shown in Fig. 5a.

The desorption peak at the initial coverage of 0.1 ML on surface Ti^{4+} is at 350 K, and the corresponding structure is methanol monomer. Interestingly, although the thermodynamic preferred structure is methanol monomer of 0.2 ML as shown in Fig. 2b, a small desorption peak appears at 310 K in Fig. 5b and can be assigned to the dimer structures, which originates from the thermodynamic equilibrium at the temperature above 0 K. These results imply that the real adsorbed methanol structure at 0.2 ML is a coexistence of dimer and monomer structures. Similarly, when the initial coverage is higher than 0.6 ML instead of 0.67 ML, a desorption peak at 155 K appears and is assigned to the full coverage (1 ML) adsorption structure.

Henderson et al. assigned the desorption peak at 295 K to molecular adsorbed methanol and the peak at 350 K to dissociated adsorption, and Guo et al. [35] found that the molecular methanol is slightly more stable than the dissociated methanol on TiO_2 surface. Therefore, the TPD of the molecular methanol on $TiO_2(110)$ is also simulated as shown in Fig. 5c. It is found that there are two strong desorption peaks at about 270 K and 325 K. Compared to the dissociated adsorption, the high-temperature desorption peaks of molecular methanol shifts to lower temperature by about 20 K due to the lower adsorption energy by DFT calculations. Two separate higher temperature peaks at 270 K and 325 K are also observed in TPD of molecular methanol on TiO_2 surface, indicating that the higher two desorption peaks are independent on whether the methanol is dissociated or not. Therefore, the desorption peak at 270 K for molecular methanol is assigned to desorption of dimer structure and the peak at 325 K is assigned to the desorption of monomer.

4 Conclusions

The structures and adsorption energies of methanol on $TiO_2(110)$ surface at different coverage are investigated. Based on DFT calculations, the dimer structure is more stable than the monomer structure at the higher coverage. According to the thermodynamical analysis at different coverage, the 2/3 ML coverage shows high stability at a very wide range of temperatures and pressures due to the high steric repulsion between the neighboring methyls. Based on simulated TPD by KMC simulation, the saturated coverage of methanol on $TiO_2(110)$ is 2/3 ML after annealing at 200 K. The 1 ML methanol is desorbed to form 2/3 ML structure at about 155 K. At 200 K, the dimer methanol is dominant and it will be destroyed to monomer structure at about 290 K. At about 350 K, the monomer methanol desorbed. The dissociated methanol on the bridge oxygen vacancy desorbs at about 490 K. These results agree well with the experimental TPD and LEED results.

Acknowledgements The authors greatly thank Dr. Zefeng Ren and Prof. Xueming Yang for fruitful discussions. This study was supported by the National Natural Science Foundation of China (Grant No. 21103165) and the Natural Science Foundation of Hebei Province (No. B2017203113). This work received financial support from the National Key R&D Program of China (2017YFB0602205, 2018YFA0208603), the National Natural Science Foundation of China (91645202), the Frontier Science Key Project of the Chinese Academy of Sciences (QYZDJ-SSW-SLH054).

References

1. Guo Q, Zhou C, Ma Z, Ren Z, Fan H, Yang X (2016) Chem Soc Rev 45(13):3701
2. Setvin M, Shi X, Hulva J, Simschitz T, Parkinson GS, Schmid M, Di Valentin C, Selloni A, Diebold U (2017) ACS Catal 7(10):7081
3. Diebold U (2003) Surf Sci Rep 48(5–8):53
4. Pang CL, Lindsay R, Thornton G (2008) Chem Soc Rev 37(10):2328
5. El-Roz M, Bazin P, Daturi M, Thibault-Starzyk F (2015) Phys Chem Chem Phys 17(17):11277
6. Yang WS, Geng ZH, Guo Q, Dai DX, Yang XM (2017) J Phys Chem C 121(32):17244
7. Xiong F, Yu YY, Wu ZF, Sun GH, Ding LB, Jin YK, Gong XQ, Huang WX (2016) Angew Chem Int Ed 55(2):623
8. Migani A, Mowbray DJ (2014) Comput Theor Chem 1040:259
9. Zhang JW, Peng C, Wang HF, Hu P (2017) ACS Catal 7(4):2374
10. Onishi H, Aruga T, Egawa C, Iwasawa Y (1988) Surf Sci 193(1):33
11. Henderson MA, Otero-Tapia S, Castro ME (1999) Faraday Discuss 114:313
12. Henderson MA, Otero-Tapia S, Castro ME (1998) Surf Sci 412–413:252
13. Bates SP, Gillan MJ, Kresse G (1998) J Phys Chem B 102(11):2017
14. Bates SP, Kresse G, Gillan MJ (1998) Surf Sci 409(2):336
15. de Armas RS, Oviedo J, San Miguel MA, Sanz JF (2007) J Phys Chem C 111(27):10023
16. Oviedo J, Sanchez-De-Armas R, Miguel MAS, Sanz JF (2008) J Phys Chem C 112(46):17737
17. Kresse G, Hafner J (1993) Phys Rev B 48(17):13115
18. Perdew JP, Zunger A (1981) Phys Rev B 23(10):5048
19. Perdew JP, Burke K, Wang Y (1996) Phys Rev B 54(23):16533
20. Blochl PE (1994) Phys Rev B 50(24):17953
21. Muscat J, Swamy V, Harrison NM (2002) Phys Rev B 65(22):224112
22. Harris LA, Quong AA (2004) Phys Rev Lett 93(8):086105
23. Grimme S, Antony J, Ehrlich S, Krieg H (2010) J Chem Phys 132(15):154104
24. Grimme S, Ehrlich S, Goerigk L (2011) J Comput Chem 32(7):1456
25. Reuter K, Scheffler M (2003) Phys Rev B 68(4):045407
26. McLeod AS, Gladden LF (1998) Catal Lett 55(1):1
27. Neurock M, Mei D (2002) Top Catal 20(1):5
28. Mei D, Hansen EW, Neurock M (2003) J Phys Chem B 107(3):798
29. Rogal J, Reuter K, Scheffler M (2008) Phys Rev B 77(15):155410
30. Hansen EW, Neurock M (2000) J Catal 196(2):241
31. Reuter K, Scheffler M (2006) Phys Rev B 73(4):045433
32. Sun KJ, Zhao YH, Su HY, Li WX (2012) Theor Chem Acc 131(2):1118
33. Liu S, Liu AA, Wen B, Zhang RD, Zhou CY, Liu LM, Ren ZF (2015) J Phys Chem Lett 6(16):3327
34. Lang XF, Liang YH, Sun LL, Zhou SX, Lau WM (2017) J Phys Chem C 121(11):6072
35. Guo Q, Xu C, Ren Z, Yang W, Ma Z, Dai D, Fan H, Minton TK, Yang X (2012) J Am Chem Soc 134(32):13366